A High-Q Terahertz Resonator for the Measurement of Electronic Properties of Conductors and Low-Loss Dielectrics

Benjamin B. Yang, *Member, IEEE*, Sarah L. Katz, Keely J. Willis, *Member, IEEE*, Marcus J. Weber, *Member, IEEE*, Irena Knezevic, *Member, IEEE*, Susan C. Hagness, *Fellow, IEEE*, and John H. Booske, *Fellow, IEEE*

***Abstract*—The successful engineering of sources and components in the terahertz (THz) regime benefits from good characterization of materials properties. Previous research reports have shown that calculations of material parameters that are valid at radio frequencies are no longer accurate at THz frequencies. A high-quality-factor quasi-optical hemispherical resonator operating between 300 GHz–1 THz has been designed and implemented for the measurement of electronic properties of conductors as well as low-loss dielectrics. This apparatus is the first quasi-optical resonator to achieve $Q \approx 4 \times 10^5$ at frequencies greater than 400 GHz in the THz regime. It is also the first open resonator designed to measure effective conductivity at these frequencies. This paper discusses the techniques that enabled high-Q operation in the THz regime. It also includes measurements of silicon with different doping densities and conductors of various surface roughness values with comparison to theoretical predictions.**

***Index Terms*—Conductivity, resonator, roughness, terahertz.**

I. Introduction

THE utilization of the terahertz (THz) or submillimeter regime of the electromagnetic spectrum is hindered by a lack of effective and convenient sources and amplifiers. Among the challenges to building these devices is the need for a validated physical model for the electronic properties of materials involved in THz system design [1]. The most fundamental materials property for many components is the complex permittivity, which consists of the relative permittivity (or refractive index) and the conductivity (or the loss tangent). These materials parameters relate directly to both the losses in a device and the functionality of a component. They are crucial in the design of next-generation sources and amplifiers, especially for vacuum electronics [2]. The relative permittivity values of most materials in the THz regime are close to their static values [3]. The conductivity, or loss tangent, proves to be more challenging to measure and predict.

While it is common knowledge that effective surface resistivity of metals is higher in the THz regime than at RF frequencies, scientists have not sufficiently characterized the relationship between THz surface resistivity, frequency, and surface characteristics to provide practical predictive capabilities [4]–[6]. While there has been good progress towards the modeling of the intrinsic surface resistivity of bulk metals [7]–[9], the exact relationship between surface roughness and effective conductivity is still unquantified. Such information is critical to the development of next-generation sources and detectors. The current microfabrication techniques used to create up-and-coming vacuum electronics devices have sidewall roughness features on the order of 50 nm, which is close to the skin depth of gold at 650 GHz [10]–[14]. Successfully characterizing the above relationships requires a means to empirically measure effective conductivity beyond 400 GHz. Such an apparatus has not been demonstrated prior to this paper.

In this paper, we demonstrate the feasibility of building a resonator at frequencies beyond 400 GHz with a sufficiently high quality factor for sensitive measurements of dielectrics and conductors. The presented apparatus is the first of its kind to measure effective conductivity over a small area at these frequencies while providing a framework to easily exchange and compare two samples. The measurement area of less than 13 mm^2 provides the unique capability to determine the conductivity of controlled submicron roughness topographies that are difficult to fabricate over large areas. This measurement area can be further decreased if the resulting larger expansion angle of the Gaussian beam is acceptable, e.g. by fabricating larger mirrors or shortening the distance between elements to minimize diffraction losses. The above features enable further ongoing research aimed at characterizing the relationship between surface roughness—including roughness resulting from nanofabricated features—and conductivity in the THz regime.

We also discuss the solutions developed to overcome the unique challenges of operating at such frequencies. The techniques presented include using a single coupling film and wire

Manuscript received January 06, 2012; revised March 01, 2012; accepted March 15, 2012. Date of publication June 28, 2012; date of current version July 12, 2012. This work was supported by the Air Force Office of Scientific Research under Grant FA9550-08-1-0052, by the Duane H. and Dorothy M. Bluemke Foundation, and by Northrup Grumann.

B. B. Yang was with the Department of Electrical and Computer Engineering, University of Wisconsin-Madison, Madison, WI 53706 USA. He is now with the Validation and Failure Analysis Department, Sandia National Laboratories, Albuquerque, NM 87185 USA.

S. L. Katz was with the Department of Electrical and Computer Engineering at the University of Wisconsin-Madison, Madison, WI 53706 USA. She is now with GE Global Research Laboratory Niskayuna, Schenectady, NY 12309 USA.

K. J. Willis was with the Department of Electrical and Computer Engineering, University of Wisconsin-Madison, Madison, WI 53706 USA. She is now with AWR Corporation, Mequon, WI 53092 USA.

I. Knezevic, S. C. Hagness, and J. H. Booske are with the Department of Electrical and Computer Engineering, University of Wisconsin-Madison, Madison, WI 53706 USA (e-mail: booske@engr.wisc.edu).

M. J. Weber was with Department of Electrical and Computer Engineering, University of Wisconsin-Madison, Madison, WI 53706 USA. He is now with the Department of Electrical Engineering, Stanford University, Palo Alto, CA 94305 USA.

Color versions of one or more of the figures in this paper are available online at http://ieeexplore.ieee.org.

Digital Object Identifier 10.1109/TTHZ.2012.2199578

grids to overcome the low ratio between the THz source power and detector sensitivity, characterizing non-negligible coupling film loss, improvements on a previously published curve-fitting technique, and an analysis of remaining sources of system error. Examples of the resonator's application are also described at 400 and 650 GHz.

In Section II, we provide a background of previous work on measuring electronic materials properties using open resonators and provide details on the design and implementation of the apparatus in this paper. In Section III, we report electrical properties of dielectrics such as silicon using the resonator system. The resonator was also used to measure conductors and the results are described in Section IV. In Section V, we summarize the results and discuss their implications.

II. Current State of the Art and the Proposed Method

A. *Existing Approaches to Measuring* THz *Electronic Properties*

Scientists and engineers have used open resonators to measure the electronic properties of materials since the 1960s [15]. Resonance peaks can be found by recording the return power while varying the frequency of the input signal that is being coupled into the resonator. The sharpness, or quality factor (Q), of the peaks correlates to the losses within the resonator, including the reflection and absorption losses of the device under test. The resonance frequencies relate to the optical path length of the resonator, which changes when the device under test is inserted.

The operating frequency of these resonators has progressively increased over the years, as new radiation sources have become available [16]–[18]. As the frequency increases past the W-band, many traditional microwave approaches become impractical. Waveguide and coaxial propagation become lossy, resulting in the need for free-space quasi-optical techniques [19], [20]. The precision required for successful iris coupling also becomes increasingly difficult beyond 100 GHz, which necessitates alternative coupling approaches such as the use of a thin coupling film. Implementing the above changes has enabled measurements via the resonator approach of dielectric constant, loss tangent, and conductivity values at frequencies beyond the W-band up to 380 GHz [19]–[21].

Time-domain spectroscopy (TDS) has been the primary approach to obtaining measurements beyond 200 GHz [22]–[24]. This technique, however, is mainly limited to low-loss samples. While reflective TDS has been demonstrated, it is difficult and very sensitive to positioning errors [25]. Time-domain spectroscopy ellipsometry (TDSE) combines TDS with ellipsometry to overcome much of the sensitivity to positioning errors but still requires a large angle of incidence to the sample due to the nature of the design [26]. The TDSE technique is being continually refined and was successfully applied to characterize thin dielectric films [27]. The resonator technique presented in this paper complements existing TDS and TDSE technology by providing the ability to perform measurements of samples at a normal incident angle. It is well-equipped to measure high-loss samples and conductors. High-loss samples can be fabricated as thin films for higher transmission and placed on the surface of one of the mirrors for structural support. Good conductors can be characterized by substituting one of the resonator mirrors for the material being measured. The combined capabilities of this resonator technique and TDSE allow the measurement of effective conductivity at a variety of angles of incidence. This ability is necessary for in-depth studies of reflection losses due to surface features that may have an angular dependence.

Building a resonator at THz-regime frequencies above 400 GHz has a unique set of challenges that do not exist below 100 GHz. The effective optical thickness of the coupling films is more than four times larger. This makes the films more reflective, causing them to couple more energy out of the resonator, which in turn lowers the quality factor and sensitivity. Using an increasingly thinner film becomes problematic because it lowers the power of the return signal. The ratio between the source power and detector sensitivity is much lower at these frequencies, primarily due to the low power of available radiation sources. Therefore, the design parameters of the resonator must fall in a narrow window where the quality factor is sufficiently high while still returning sufficient power to the detector. This restriction typically means that, unlike previous resonators, the coupling film is thick enough to have a non-negligible loss that must be taken into account when evaluating Q.

B. *Overview of Proposed Method*

Fig. 1 gives an overview of the resonator system described in this paper. The THz source consists of a microwave frequency synthesizer connected to an amplifier multiplier chain (AMC). The AMC up-converts the signal from the synthesizer by a large factor into the THz regime. For the examples described in this paper, two AMCs up-converts the synthesizer signal by factors of 36 or 48 to produce a frequency at 400 or 650 GHz, respectively, and an operating bandwidth of 4 GHz. The signal is polarized horizontally such that it passes through the vertical wire grid. The two focusing mirrors reshape the beam for optimal coupling into the resonator. Due to the 45-deg wire grid, the polarization of the signal coupled into the resonator is at a 45-deg angle compared to the initial output of the AMC.

As the THz signal travels between the two resonator mirrors, a fraction of the power is reflected back out into the elliptical focusing mirrors and through the 45-deg wire grid. The vertical wire grid separates the return signal from the input signal and sends half of the return signal to the Golay cell. The sensitivity of the Golay cell is enhanced by a lock-in amplifier, allowing it to detect signals below 100 nW.

The variation of the input frequency, ν, over the range of the AMC allows identification of periodic cavity resonance peaks in the return signal at the Golay cell detector. The distance between peaks, $\Delta\nu$, is equal to $c/(2L)$, where c is the speed of light and L is the resonator length (the distance between the two mirrors). This relationship provides an initial assessment of the resonator length.

$P(\nu)$ is found by curve-fitting a Lorentzian function to the data points [28]

$$P(\nu) = \frac{C_1}{\pi C_2 \left[1 + \left(\frac{\nu - C_3}{C_2}\right)^2\right]} + C_4 \tag{1}$$

where $P(\nu)$ is the measured return power, and C_1, C_2, C_3, and C_4 are curve-fit parameters. C_2 represents the half-width-at-half-maximum (HWHM), or one-half of the full-width-at-half-

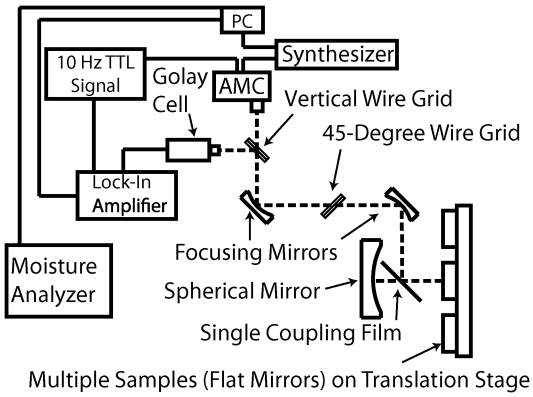

Fig. 1. Schematic of the resonator system. The AMC emits THz radiation that is reshaped by the focusing mirrors and coupled into the resonator through a single coupling film. The resonator consists of two mirrors: the diamond-turned copper mirror and the device under test, which serves as a flat mirror. While the signal travels between the two mirrors, the coupling film reflects a fraction of it back through the focusing mirrors. A series of wire grids placed along the return path directs a portion of the return signal to the Golay cell, whose sensitivity is enhanced by the lock-in amplifier. The moisture analyzer monitors the humidity to ensure that atmospheric propagation losses are successfully minimized by the desiccants and sealed enclosure surrounding the apparatus.

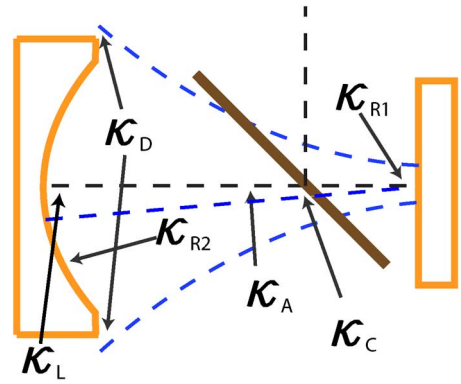

Fig. 2. Definition of various sources of losses within the resonator.

maximum (FWHM) of the peak. C_3 is equal to the center frequency, ν_C. C_4 corresponds to the broadband noise. C_1 is related to the peak power at the resonant frequency, $P_{\max}$, by $C_1 = \pi C_2(P_{\max} - C_4)$.

There has been a previous report of an iterative approach producing good three-parameter curve fits to the equation above—without the C_4 term—when the signal-to-noise ratio is low [29]. Additional experimentation revealed that a similar effect can be found by adding in a fourth parameter, C_4, to represent the broadband noise. We found the four-parameter curve fit to be more efficient and robust than an iterative, three-parameter curve fit. Once the curve fit is complete, the key characteristics needed to determine relative permittivity and effective conductivity can be extracted from the curve fit parameters:

$$\nu_c = C_3 \quad \text{(center frequency)} \tag{2a}$$

$$Q = \frac{\nu_c}{\nu_{\text{FWHM}}} = \frac{C_3}{2C_2} \quad \text{(quality factor)} \tag{2b}$$

where ν_{FWHM} represents the FWHM.

Multiple measurements and curve fits are performed for the data in this study, and the standard deviation of each measurement is tracked and logged. The measured quality factor, Q_{tot}, is related to the individual sources of loss in the resonator by the following relationship:

$$\frac{1}{Q_{\text{tot}}} = \sum_{i=1}^{n} \frac{1}{Q_i} = \frac{c}{2\pi\nu_c L} \sum_{i=1}^{n} \kappa_i \tag{3}$$

where κ_i is the fractional loss that the signal experiences during a one-way trip. Fig. 2 visually summarizes the various sources of loss considered during the design of the resonator system: losses due to diffraction (κ_D), misalignment (κ_L), atmospheric scattering and absorption (κ_A), the coupling film (κ_C), and reflection losses due to the surface impedance of the two mirrors (κ_{R1} and κ_{R2}).

In order to have maximum sensitivity to changes in one-way loss when a sample is incorporated in the resonator, all sources of loss must be made as small as possible relative to the reflection losses of the mirror (κ_{R1} and κ_{R2}). The losses due to diffraction have been made negligible in the design phase by ensuring that the diameter of both mirrors exceed four times the $1/e$ radius, resulting in a one-way trip loss of two orders of magnitude smaller than κ_{R1} and κ_{R2}. The loss due to misalignment has also been minimized through the addition of alignment pins on almost all of the components. The remaining parts that cannot incorporate alignment pins have optical mirrors mounted on key surfaces, allowing alignment with the aid of a visible laser. The resulting angular misalignment in the resonator system is less than 2 mrad, making κ_L much smaller than κ_{R1} and κ_{R2}.

Water content is the primary source of atmospheric loss (κ_A). In order to minimize water-content, a hermetically-sealed enclosure was built around the system with electrical feed-through ports and moisture analyzers. The inclusion of molecular sieve desiccant brings the water content in the enclosure down to between 50–100 parts-per-million by volume (ppmV). Measurements and model predictions [30] demonstrate propagation losses within this range are insignificant compared to the remaining sources of loss.

As mentioned previously in this paper, successful operation at 400 GHz and above requires a balance between a high quality factor and strong return signal. One of the initial challenges was the thick coupling film required to produce a detectable return signal. Initial calculations found that the separate input and output coupling films used in W-band resonators [19] would raise the coupling loss, κ_C, and lower the quality factor beyond the required value for sensitive conductivity measurements. This is because at 650 GHz, the coupling films are optically thicker to the THz signal than a W-band one, resulting in a higher κ_C. The resonator design overcame this challenge by having a single 5-μm polytetrafluoroethylene (PTFE) film serve as both the input and output coupling films, which halves the coupling film loss. The vertical and 45-degrwire grids direct a portion of the return signal towards the Golay cell detector at the cost of a 75% round-trip loss.

Unfortunately, even with these improvements, the 5-μm PTFE film still results in a non-negligible κ_C when compared to κ_{R1} and κ_{R2}. Unlike resonators operating at lower frequencies, where the solution is to use ever-thinner films at the cost of a weaker return signal, the current system is prohibited from

doing so due to the low output power (<1 mW) available at 400 and 650 GHz. As such, characterization of κ_C is necessary.

Experimental measurements validated initial theoretical estimates of κ_C, κ_{R1} and κ_{R2}. First, care was taken such that the planar and spherical mirrors were manufactured from the same slab of bulk oxygen-free copper using the same diamond-turning technology so that they had similar surface features and chemical compositions. Both diamond-turned copper mirrors were characterized using an interferometer to have an RMS roughness of less than 6 nm—less than 1/10 of the skin depth of copper at 650 GHz—ensuring minimal reflection losses compared to any device under test that is subsequently inserted. These efforts ensured that both mirrors have a similar effective conductivity, and thus

$$\kappa_{R1} \approx \kappa_{R2} = \kappa_R^{Cu}. \tag{4}$$

By treating the thin coupling films as a dielectric slab with material properties from published measurements [3] and taking into account multiple reflections, the ratio of the coupling loss between a 5-μm and 10-μm PTFE film was established ($\kappa_C = \kappa_C^5$ or κ_C^{10}) [31]

$$\kappa_C^{10} = M\kappa_C^5 \tag{5}$$

where

$$M = 3.97 \quad \text{at } 400 \text{ GHz} \tag{6a}$$
$$M = 3.93 \quad \text{at } 650 \text{ GHz}. \tag{6b}$$

The quality factor using both coupling film thicknesses (Q_m^5 for the 5 μm-thick film and Q_m^{10} for 10 μm-thick film) were measured at both 400 and 650 GHz. Given that $\kappa_{R1} \approx \kappa_{R2} = \kappa_R^{\text{Cu}}$ and $\kappa_D, \kappa_L, \kappa_A \ll \kappa_C, \kappa_R^{\text{Cu}}$, (3), (5), (6a) and (6b) can be rewritten to provide a system of two equations and two unknowns for each frequency

$$\kappa_R^{Cu} + \kappa_C^5 = \frac{2\pi\nu L}{cQ_m^5} \tag{7}$$
$$\kappa_R^{Cu} + M\kappa_C^5 = \frac{2\pi\nu L}{cQ_m^{10}}. \tag{8}$$

Solving this system of two equations provides a value for both the coupling loss of the 5-μm film as well as the effective conductivity of the diamond-turned mirrors. Measurements of Q_m^5 and Q_m^{10} resulted in κ_C^5 and κ_C^{10} that were within 5% of the expected calculated thin-film values using published dielectric constants [3], [31]. This information enabled the measurement of absolute, instead of relative, effective conductivity values of metal samples using a process described in Section IV.

With κ_C, κ_{R1}, and κ_{R2} characterized and all other sources of loss made negligible, (3) can be written as

$$\frac{1}{Q_{\text{tot}}} = \frac{c}{2\pi\nu L}\left[\kappa_C + \frac{1}{2}(\kappa_{R1} + \kappa_{R2})\right]. \tag{9}$$

The resonator can then be used to measure properties of low-loss dielectrics or semiconductors and metals by inserting the sample as depicted in Fig. 3. The information can then be extracted from a comparison with the unloaded case, where the diamond-turned spherical and flat mirrors are used. The sample with the highest loss loaded into the resonator that still provided

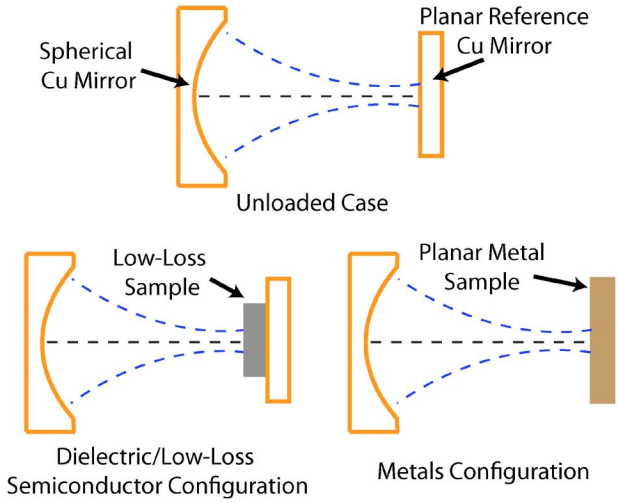

Fig. 3. Various configurations of the resonator.

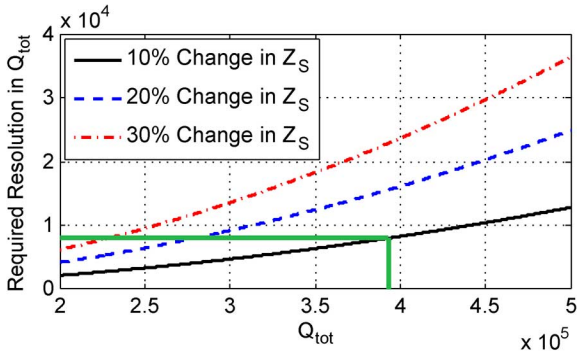

Fig. 4. The calculated quality factor resolution necessary in order to detect a 10%, 20% and 30% change in the surface resistance, Z_S, as a function of the unloaded quality factor, Q_{tot}. The plot shows that the existing Q of 3.9×10^9 and resolution of approximately 10^4 is sufficient to detect a roughly 10% change in surface resistance.

a detectable return signal produced a Q corresponding to a 4.7% one-way fractional power loss. This result provides an approximate upper limit to the amount of acceptable loss for a dielectric sample or reflecting conductor before necessitating further pre-measurement processing, such as applying a thicker coupling film at the expense of lower Q and sensitivity or thinning the dielectric sample.

The resolution in measured effective conductivity depends mostly on the resolution of the measured Q. The characterization process of the resonator found a nominal unloaded $Q = 3.9 \times 10^5$ with a repeatability of just under 1×10^4. Fig. 4 shows the change in Q_{tot} in (9) when the flat mirror's surface impedance, κ_{R1}, changes by 10%, 20%, and 30%. The Q resolution is sufficient to detect an approximately 10% change in the surface impedance of the sample. The sensitivity increases if the sample has a conductivity much lower than the diamond-turned copper mirror, since it becomes the dominating κ_i in (3).

The specified fabrication tolerances, such as deviation in curvature of the spherical mirror and distance to the planar mirror, have negligible effects on the radiation power, relative frequency shift, and quality factor of the resonance curves. The measured resonator loss matches the expected value due to

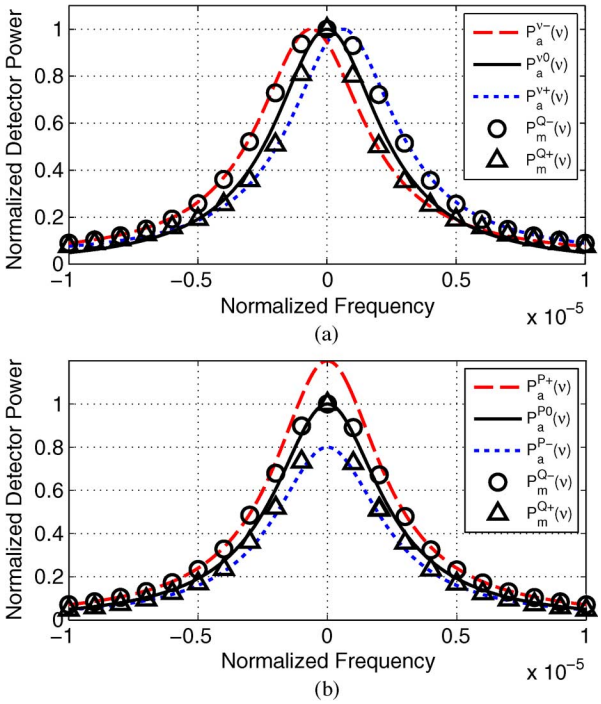

Fig. 5. Variation in measured quality factor due to two potential causes: (a) shifts in the center frequency from $P_a^{\nu-}(\nu)$ to $P_a^{\nu+}(\nu)$ caused by a change in resonator length during the resonance scan can cause an error in the inferred Q; (b) changes in the power of the radiation source during a resonance scan from $P_a^{P0}(\nu)$ to either $P_a^{P+}(\nu)$ or $P_a^{P-}(\nu)$ can cause an error in the inferred Q. In both (a) and (b), the circles of $P_a^{Q-}(\nu)$ illustrate a case where the apparent measured line width is broader than the actual one, resulting in a lower Q. The triangles of $P_a^{Q+}(\nu)$ illustrate a case where the measured line width is narrower the actual one, resulting in a higher Q.

mirror reflection and coupling film loss alone. This correlation shows that primary contributors to the measured Q are the reflection and coupling film loss, not fabrication errors.

A sensitivity analysis shows that the above fabrication errors can change the Q by ≈1/10 of the measured repeatability of 1×10^4. Therefore, a closer look at other causes of the observed repeatability is warranted. Assuming that the losses in the resonator are steady during the resonance peak measurement, the other principle candidate sources of the 1×10^4 observed variation in Q are instabilities in either the resonator length or AMC signal strength. The following two subsections provide a quantitative exploration to establish these two factors as reasonable causes of the observed uncertainty.

C. Sources of Uncertainty: Resonator Length

A change in resonator length during data acquisition alters the center frequency of the peak, which can cause the measured peak to become broader or narrower than the actual one. Fig. 5(a) illustrates this concept. The various lines represent Lorentzian curves with the same quality factor but different center frequencies. Depending on whether the frequency is shifting to the left or the right during measurement, the observed quality factor can be lower (circular data points in the figure) or higher (triangle data points) than the actual value.

An estimation of the change in resonator length that results in the observed uncertainty can be derived by examining the Lorentzian in (1). Since the signal-to-noise ratio of typical measurements is approximately 10:1, we focus on the broadening at the point where the power has dropped to 1/10 of its maximum value, or the full-width-at-1/10-maximum points. By setting $P(\nu) = P_{\max}/10$ and solving for the frequency, ν, it can be found that this power occurs at a frequency $(3 \times \mathrm{HWHM})$ from the center frequency.

To model the broadening, suppose that the system has an actual frequency response of $P_a(\nu)$, with a quality factor of Q_a and HWHM of HWHM_a. During measurement, the center frequency shifts from ν_c to $\nu_s = \nu_c + \delta\nu$, resulting in an observed frequency response of $P_m^{Q-}(\nu)$. This measured $P_m^{Q-}(\nu)$ has an erroneously lower Q of Q_m and HWHM of HWHM_m compared to the actual value. The transition from the $P_a^{\nu-}(\nu)$ curve to the $P_a^{\nu+}(\nu)$ curve in Fig. 5(a) represent the actual frequency response, $P_a(\nu)$, with frequency shifts during measurement. The circles of $P_m^{Q-}(\nu)$ in Fig. 5(a) represent the measured frequency response that is erroneously broadened. This shift in the center frequency can result from a resonator length shift of δL during measurement:

$$\delta L = \frac{c}{2}\left(\frac{1}{\nu_c} - \frac{1}{\nu_s}\right). \tag{10}$$

As the Lorentzian fit incorporates all data points above the noise level (between full-width-at-1/10-maximum points), it can be shown that the measured HWHM_m will be larger than the actual HWHM_a by:

$$\mathrm{HWHM}_m = \mathrm{HWHM}_a + \frac{\delta\nu}{3} \tag{11}$$

resulting in a Q_m that can be compared with the actual quality factor, Q_a, using (2b)

$$Q_a = \frac{\nu_c}{2\mathrm{HWHM}_a} \tag{12}$$

$$Q_m = \frac{\nu_c + \left(\frac{1}{2}\right)\delta\nu}{2\mathrm{HWHM}_a + \left(\frac{2}{3}\right)\delta\nu}. \tag{13}$$

Comparing the numerators and denominators confirms that Q_m is indeed smaller than Q_a. A similar analysis with a change in algebraic signs applies to the case where the center frequency shifts to a smaller value during measurement $(\nu_s = \nu_c - \delta\nu)$ yielding an erroneously smaller value of HWHM_m and thus a higher Q_m. This scenario is illustrated by the triangular data points of $P_m^{Q+}(\nu)$ in Fig. 5(a).

The above equations suggest that a change in resonator length on the order of 110 nm is sufficient to result in the observed Q uncertainty of 1×10^4. The resonator is mounted onto a standard optical table that is primarily made of stainless steel. Using a typical thermal expansion coefficient for stainless steel of 10.4 μm/°C [32], the temperature change required for a resonator length drift of 110 nm is a mere 0.011 °C.

Each measurement of a resonant peak takes between 30 min to 1 h, depending on the measurement parameters. The temperature in the room housing the experiment is not tightly controlled and the ambient temperature can change as much as 1 °C over the course of a series of measurements. Therefore, it is reasonable to suggest that the core temperature of the table could drift

by the 0.011 °C necessary to create the observed uncertainty in Q during a single resonance scan.

D. Sources of Uncertainty: AMC Power

Power fluctuations in the AMC signal source can also result in a measured Q that is higher or lower than the actual value. Fig. 5(b) illustrates this concept by plotting multiple Lorentzian curves of identical quality factors but differing maximums. Again, taking measurements as the system varies between the different power levels can result in measured Qs that are lower (circular data points of $P_m^{Q-}(\nu)$ in the figure) or higher (triangle data points of $P_m^{Q+}(\nu)$) than the actual value.

First, we define two curves: $P_a^{P0}(\nu)$, illustrated in Fig. 5(b), corresponds to the actual frequency response of the system and takes the form of (1), where $C_2 = \mathrm{HWHM}_a$, or the actual HWHM. It has a quality factor of Q_a, which is related to C_2 by (2b). We also define $P_m^{Q-}(\nu)$, which corresponds to a measured frequency response that has an erroneously lower quality factor, $Q_m < Q_a$, and is represented by the circles in Fig. 5(b). Its HWHM, HWHM_m, is also related to C_2 by (2b). Both curves have peaks centered at ν_c.

We set $Q_a = 3.9 \times 10^5$, which is the nominal, unloaded Q of the system. Since the observed repeatability is 1×10^4, we let Q_m represent a worst-case measurement at the limits of the observed uncertainty, or $Q_m = 3.85 \times 10^5$. These values, along with the information in the previous paragraph, gives the parameters to define $P_a^{P0}(\nu)$ and $P_m^{Q-}(\nu)$.

To correlate with the observed signal-to-noise ratio, emphasis is again placed at the full-width-at-1/10-maximum points, or $3 \times \mathrm{HWHM}$ from the center frequency. The power fluctuation that would result in the observed uncertainty can be calculated by finding the fractional power difference, $\delta P/P$, at the point of interest

$$\frac{\delta P}{P} = \frac{P_m^{Q-}(\nu_c - 3\times\mathrm{HWHM}_m) - P_a^{P0}(\nu_c - 3\times\mathrm{HWHM}_a)}{P_a^{P0}(\nu_c - 3\times\mathrm{HWHM}_a)}. \tag{14}$$

Evaluating (14) with the above values shows that a power drift on the order of $\delta P/P \approx 2\%$ is sufficient to result in the observed 1×10^4 variation in Q. A similar analysis leading to the same result can be performed with $Q_m = 3.95 \times 10^5$, which corresponds to power fluctuations resulting in an erroneously higher Q, as illustrated by the triangular points of P_m^{Q+} in Fig. 5(b). In order to minimize the effects of environmental variations and obtain several measurements in a reasonable length of time, it is necessary to step the frequency every 10–20 s. The AMC potentially has not had sufficient time to thermally stabilize during this time. Therefore, it is reasonable to hypothesize that the AMC output power is varying by the 2% necessary to cause the observed variation in measured Q.

III. Measurements of Low-Loss Dielectrics

The theory behind measuring low-loss (i.e. THz transmission greater than ≈97%) dielectrics with the resonator approach is outlined by Yu and Cullen [33]. A comparison of the resonance peaks measured in the unloaded case and the dielectric/low-loss semiconductor configuration shown in Fig. 3 allows extraction of the dielectric constant and loss tangent. The insertion of a low-loss dielectric sample changes the effective optical path length of the resonator as well as the single-pass loss compared to the unloaded case.

The first step in measuring the relative permittivity is to obtain a good estimate of the unloaded resonator length, L, so that the exact mode number of the resonance can be determined. An initial estimation of L can be made by finding the center frequencies of multiple resonance peaks and relating the peak spacing, $\Delta\nu$, to the resonator length

$$\Delta\nu = \frac{c}{2L} \tag{15}$$

where c is the speed of light in the propagation medium. The resulting L can be further improved by using it as an initial guess to numerically solve a more accurate equation for the resonant frequency ν_u [33]

$$\nu_u = \frac{c}{4L}\left[q + 1 + \frac{1}{\pi}\arccos\left(1 - \frac{2L}{R_m}\right) - \frac{1}{2\pi\beta_u R_m}\right] \tag{16}$$

where q is the mode number, R_m is the curvature radius of the spherical mirror, and $\beta_u = 2\pi\nu_u/c$ is the wave number corresponding to the unloaded resonance frequency, ν_u.

Once the measurement for the unloaded case is complete, the low-loss sample is attached to the flat mirror as shown in the low-loss dielectric/semiconductor configuration in Fig. 3. After recording the new peak frequencies and quality factors, the relative permittivity can be found by solving the transcendental [18]

$$\frac{1}{n}\tan(n\beta_L t - \Phi_T) = -\tan(\beta_L d - \Phi_D) \tag{17}$$

where

$$\Phi_D = \arctan\left(\frac{d + \frac{t}{n}}{z_L}\right) - \arctan\left(\frac{1}{\beta_L R_m}\right) - \arctan\left(\frac{t}{nz_L}\right) - \arctan\left(\frac{1}{\beta_L R_2(t)}\right)$$

$$\Phi_T = \arctan\left(\frac{t}{nz_L}\right) - \arctan\left(\frac{1}{n\beta_L R_1(t)}\right)$$

$$R_1(t) = t + \frac{n^2 z_L^2}{t}$$

$$R_2(t) = \frac{t}{n} + \frac{nz_L^2}{t}$$

and

- d distance between sample and spherical mirror;
- t thickness of sample;
- n initial guess for sample refractive index;
- ν_L loaded resonance frequency;
- $\beta_L = 2\pi\nu_L/c$;
- $z_L = \sqrt{(d')(R_m - d')}$;
- $d' = d + (t/n)$.

In order to solve the transcendental equation, an initial guess for the refractive index is necessary. For this purpose, a known value at the closest frequency possible is an adequate initial guess. In most cases the variation of the refractive index as a function of frequency is small enough to allow the numerical solver to arrive at the correct local solution.

TABLE I
COMPARISON OF MEASURED VALUES OF RELATIVE PERMITTIVITY WITH VALUES FROM LITERATURE [3]

Sample Material	Measured Relative Permittivity (ϵ_r)	Relative Permittivity in Literature (ϵ_r) [3]
Single-Crystal Quartz	4.60 ± 0.04	4.64
Silicon	11.89 ± 0.02	11.88

This approach has been used to successfully measure the relative permittivity ($\epsilon_r = n^2$) for a silicon and quartz sample. Uncertainty in the sample thickness is the primary source of error in both cases. Table I summarizes the resulting measured values compared with those cited in [3].

The resonator can also be used to determine the loss tangent or conductivity of the low-loss sample. By measuring the quality factor of the unloaded resonator, Q_U, and the loaded resonator, Q_L, the effective quality factor due to the additional losses from the dielectric Q_ϵ can be calculated

$$\frac{1}{Q_\epsilon} = \frac{1}{Q_L} - \frac{1}{Q_U}. \tag{18}$$

By correlating Q_ϵ to the fractional loss-per-pass we can calculate loss tangent of the sample [33]

$$\tan\delta = \frac{2n\beta_L(d+t\Delta)}{Q_\epsilon\left[2n\beta_L t\Delta - \Delta sin(2n\beta_L t - 2\Phi_T)\right]} \tag{19}$$

where

$$\Delta = \frac{n^2}{n^2\cos^2(n\beta_L t - \Phi_T) + \sin^2(n\beta_L t - \Phi_T)}. \tag{20}$$

The conductivity, σ, of the sample relates to the loss tangent $\tan\delta$ by

$$\sigma = 2\pi\nu_L n^2 \epsilon_0 \tan\delta. \tag{21}$$

The resonator has also been used to measure silicon samples of different doping densities for comparison with a self-consistent ensemble Monte Carlo/finite-difference time-domain (EMC/FDTD) simulation tool [34]–[36]. The EMC/FDTD tool has been benchmarked with past TDS measurements of silicon wafers [37]. The results are also compared with predictions from the Drude model, which describes the behavior of conductors and semiconductors at lower frequencies [38]

$$\sigma(\nu) = \frac{\sigma_{DC}}{1 + j2\pi\nu\tau} \tag{22}$$

where σ_{DC} is the conductivity for the dc case, $\sigma(\nu)$ is the frequency-dependent conductivity, and τ is the characteristic scattering time. The results of these measurements are shown in Figs. 6 and 7.

The EMC/FDTD results show a closer match to the measured values than the predictions by the Drude model, especially at higher doping densities. The increasing deviation between the EMC/FDTD simulation and the Drude model at higher doping densities further motivates developing the EMC/FDTD approach as the physics model of choice for high-conductivity materials in the THz regime.

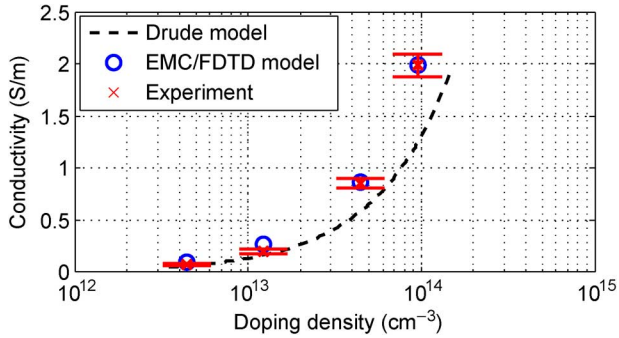

Fig. 6. Measured conductivity values compared with EMC/FDTD simulation results and Drude model predictions at 400 GHz.

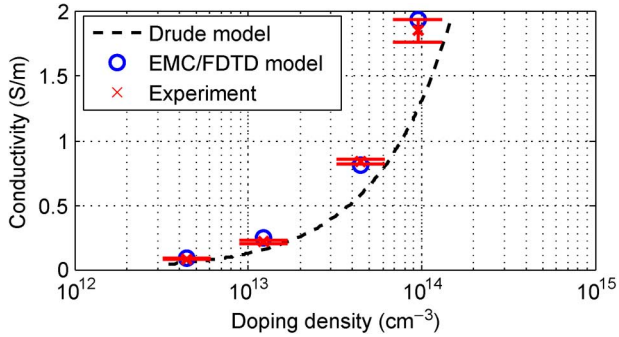

Fig. 7. Measured conductivity values compared with EMC/FDTD simulation results and Drude model predictions at 650 GHz.

IV. MEASUREMENTS OF GOOD CONDUCTORS

Another primary application of the resonator is to measure the THz conductivity of metals with sub-micron roughness features. The effective THz conductivity of a planar, metallic sample can be found by substituting it in place of the reference copper mirror as shown in the metals configuration in Fig. 3. The change in quality factor when compared to the unloaded case of Fig. 3 directly correlates to the difference in reflection losses of the substituted flat copper mirror. Since all other sources of loss are characterized, the reflection loss of the sample, and thus the effective conductivity, can be extracted.

As described in Section II-B, the atmospheric (κ_A), diffraction (κ_D), and alignment (κ_L) losses have been made negligible compared to the remaining sources of loss in Fig. 2. The measured quality factor, Q_{tot}, of the resonator can therefore be approximated by (9), repeated here for convenience:

$$\frac{1}{Q_{\mathrm{tot}}} = \frac{c}{2\pi\nu_c L}\left[\kappa_C + \frac{1}{2}(\kappa_{R1} + \kappa_{R2})\right]$$

where ν_c is the resonant frequency and L is the resonator length that can be found by using (15) as a starting point. κ_C is the coupling loss, which is a known quantity from the cavity characterization performed in Section II-B. κ_{R1} and κ_{R2} represent the reflection losses in the spherical and planar mirror, respectively. The cavity characterization of Section II-B also provided the value for the resistive loss of the spherical mirror ($\kappa_{R1} = \kappa_R^{Cu}$).

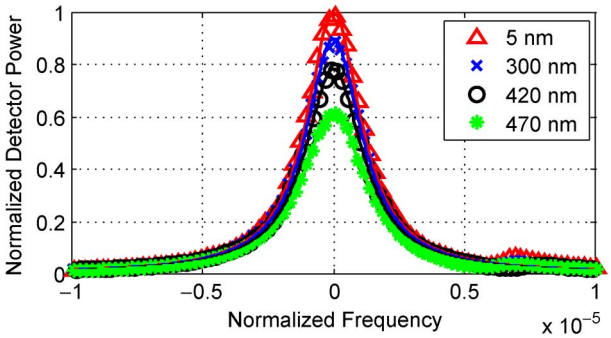

Fig. 8. Normalized measured peaks for different lapped copper planar mirror samples.

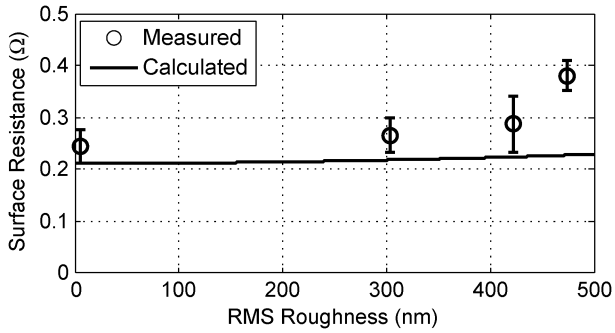

Fig. 9. Measured surface resistance of different lapped samples with different average roughness features.

By replacing the flat mirror with a planar sample of unknown conductivity and resistive loss ($\kappa_{R2} = \kappa_R^S$) (9) becomes:

$$\frac{1}{Q_{\text{tot}}} = \frac{c}{2\pi\nu_c L}\left[\kappa_C + \frac{1}{2}\left(\kappa_R^{\text{Cu}} + \kappa_R^S\right)\right]. \tag{23}$$

Solving (23) reveals the value of κ_R^S

$$\kappa_R^S = 2\left[\frac{2\pi\nu_c L}{Q_{\text{tot}} c} - \kappa_C\right] - \kappa_R^{Cu}. \tag{24}$$

Once the effective loss of the sample, κ_R^S, is found, the effective conductivity, σ_S, of the sample can be calculated with the following [6]

$$\sigma_S = \frac{16\pi\nu_c\epsilon}{\left(\kappa_R^S\right)^2}. \tag{25}$$

Depending on the resonator length after sample insertion, there are three to four resonance peaks in the usable 4 GHz bandwidth of the AMCs. To ensure repeatability, each peak was measured three times for each sample for a total of nine to twelve scans at a resolution of $\Delta\nu = 0.144$ MHz. Choice of the frequency resolution is important for accuracy. A resolution that is too fine can result in data sampling over too long a time frame and degrade measurement accuracy due to drifting conditions such as temperature fluctuations. If the resolution is too coarse, then the accuracy of the Lorentzian curve fit and the extraction of the quality factor is potentially compromised. Through trial-and-error, an optimal frequency step size that provided consistent curve fit results while performing the scan as quickly as possible was found.

The resonator was used to measure the effective THz conductivity at 650 GHz of copper samples that were machined to different root mean square (RMS) roughness values. Fig. 8 shows typical normalized resonance peak measurements of the resonator with different samples acting as the planar mirror. The legend shows the planar mirror RMS roughness values. As expected, the maximum power decreases and the peak broadens with increased roughness in the planar mirror.

Fig. 9 shows the effective surface resistance extracted from repeated measurements of multiple peaks that were curve-fitted to the Lorentzian using the techniques described in Section II-B. The experimental results are compared with a model by Saillard and Maystre for rough surface scattering [39]. Using an integral theory approach, they derived a relationship between the RMS roughness of a metal surface, ξ, and the reflectivity, R_{mi}^r, for normal incidence:

$$R_{mi}^r = R_{mi}^s e^{(-4\pi\nu\xi/c)^2}. \tag{26}$$

The smooth-surface reflectivity, R_{mi}^s can be directly calculated using the predicted surface resistance values of the classical relaxation-effect model [4], which should be valid at this frequency [7]. The surface impedance, Z_S, can be written as

$$Z_S = \sqrt{\frac{j\omega\mu}{\sigma_R + j\omega\epsilon}}$$
$$\sigma_R = \frac{\sigma_{DC}}{1 + j\omega\tau} \tag{27}$$

where ω is the frequency in radians per second, σ_{DC} is the bulk direct current (DC) conductivity of copper, and τ is the known carrier scattering rate of the metal [4].

The measurements show a reasonable agreement for a smooth surface. As the roughness increases, however, the surface resistance increases more sharply than the model predictions. While the model has been verified at 120–140 GHz [40], the deviations at 650 GHz suggest that further exploration of roughness effects on THz conductivity is warranted at higher frequencies.

V. Conclusion

The quasi-optical resonator system in this paper pushes the frequency boundaries of a resonator approach to measuring dielectric and conductor properties beyond 400 GHz. Several changes from lower frequency designs were necessary to obtain a sufficiently high quality factor for sensitive measurements of effective conductivity, such as the combination of the AMC and Golay cell with a lock-in amplifier, the implementation of the single coupling film with wire grids, and reformulation to incorporate non-negligible coupling film loss. The resulting apparatus can measure effective conductivity with an accuracy of 10% or better.

While the apparatus in this paper demonstrates operating frequencies of 400 and 650 GHz, the principles of the technique can be implemented beyond 1 THz. The primary limitation is the availability of an adequately powerful radiation source and a sufficiently sensitive detector to overcome the $\approx 10^4$ insertion loss. This loss can be decreased through the use of thicker coupling films, though it is at the expense of the quality factor and measurement sensitivity.

The resonator was used to measure silicon with doping densities between 10^{12} and 10^{14} cm^{-3} with good agreement to a benchmarked EMC/FDTD model. A disagreement with the Drude model was found with increased doping density, establishing the EMC/FDTD approach as the model of choice in the THz regime.

Measurements of copper surfaces with sub-micron surface roughness values were performed at 650 GHz and compared with theory. While a good agreement was found for smoother surfaces, the theory was a poor predictor of surface conductivity with increased roughness. The reason for this discrepancy is not well understood at this time and is the subject of future study.

The results in this paper not only indicate a need for further characterization of the effects of surface roughness on conductivity in the THz regime but also demonstrates that the resonator in this paper is a capable instrument for such studies. The small measurement region of this setup makes it the ideal tool to examine samples with nanofabricated textures using techniques such as electron beam lithography that become very expensive when patterning over large areas.

ACKNOWLEDGMENT

The authors would like to thank R. Heidinger of the Karlsruhe Institute of Technology for sharing his experiences with submillimeter resonator design. They would also like to thank Thomas Keating Instruments, the University of Wisconsin-Madison Physical Sciences Laboratory and II-VI Infrared for their assistance in machining various components.

REFERENCES

[1] P. Siegel, "Terahertz technology," *IEEE Trans. Microw. Theory Techn.*, vol. 50, no. 3, pp. 910–928, 2002.

[2] J. H. Booske, "Plasma physics and related challenges of millimeter-wave-to-terahertz and high power microwave generation," *Phys. Plasmas*, vol. 15, no. 5, p. 055502, 2008.

[3] J. W. Lamb, "Miscellaneous data on materials for millimetre and submillimetre optics," *Int. J. Infrared Millim. Waves*, vol. 17, no. 12, pp. 1997–2034, 1996.

[4] S. Lucyszyn, "Investigation of anomalous room temperature conduction losses in normal metals at terahertz frequencies," *Proc. IEE Microw., Antennas Propag.*, vol. 151, no. 4, pp. 321–329, 2004.

[5] N. Laman and D. Grischkowsky, "Reduced conductivity in the terahertz skin-depth layer of metals," *Appl. Phys. Lett.*, vol. 90, no. 12, p. 122115, 2007.

[6] P. F. Goldsmith, *Quasioptical Systems*, 1st ed. New York: Springer, Feb. 1998.

[7] S. Lucyszyn, "Evaluating surface impedance models for terahertz frequencies at room temperature," *Progr. Electromagn. Res.* , vol. 3, no. 4, pp. 554–559, 2007.

[8] B. Podobedov, "Resistive wall wakefields in the extreme anomalous skin effect regime," *Physical Review Special Topics-Accelerators and Beams*, vol. 12, no. 4, p. 044401, Apr. 2009.

[9] S. Lucyszyn and Y. Zhou, "Engineering approach to modelling metal THz structures," *THz Sci. Technol.*, vol. 4, no. 1, pp. 1–8, Mar. 2011.

[10] Y. Shin, G. Park, G. P. Scheitrum, and B. Arfin, "Novel coupled-cavity TWT structure using two-step LIGA fabrication," *IEEE Trans. Plasma Sci.*, vol. 31, no. 6, pp. 1317–1324, Dec. 2003.

[11] Y. Shin, L. R. Barnett, D. Gamzina, N. C. Luhmann, M. Field, and R. Borwick, "Terahertz vacuum electronic circuits fabricated by UV lithographic molding and deep reactive ion etching," *Appl. Phys. Lett.*, vol. 95, no. 18, p. 181505, 2009.

[12] S. Sengele, H. Jiang, J. Booske, C. Kory, D. van der Weide, and R. Ives, "Microfabrication and characterization of a selectively metallized W-Band Meander-Line TWT circuit," *IEEE Trans. Electron Devices*, vol. 56, no. 5, pp. 730–737, May 2009.

[13] Y. Shin, D. Gamzina, L. R. Barnett, F. Yaghmaie, A. Baig, and N. C. Luhmann, "UV lithography and molding fabrication of ultrathick micrometallic structures using a KMPR photoresist," *J. Microelectromech. Syst.*, vol. 19, no. 3, pp. 683–689, Jun. 2010.

[14] Y. Shin, A. Baig, L. R. Barnett, W. Tsai, and N. C. Luhmann, "System design analysis of a 0.22-THz sheet-beam traveling-wave tube amplifier," *IEEE Trans. Electron Devices*, vol. 59, no. 1, pp. 234–240, Jan. 2012.

[15] W. Culshaw and M. Anderson, "Measurement of permittivity and dielectric loss with millimetre-wave Fabry-Perot interferometer," *Proc. Inst. Elect. Eng. B—Electron. Commun. Eng.*, vol. 109, no. 23, pp. 820–826, 1962.

[16] J. Mazierska, M. V. Jacob, A. Harring, J. Krupka, P. Barnwell, and T. Sims, "Measurements of loss tangent and relative permittivity of LTCC ceramics at varying temperatures and frequencies," *J. Eur. Ceramic Soc.*, vol. 23, no. 14, pp. 2611–2615, 2003.

[17] T. E. Harrington, J. Wosik, and S. A. Long, "Open resonator mode patterns for characterization of anisotropic dielectric substrates for HTS thin films," *IEEE Trans. Appl. Supercond.*, vol. 7, no. 2, pp. 1861–1864, Jun. 2002.

[18] M. N. Afsar, X. Li, and H. Chi, "An automated 60 GHz open resonator system for precision dielectric measurements," *IEEE Trans. Microw. Theory Techn.*, vol. 38, no. 12, pp. 1845–1853, Dec. 2002.

[19] M. Thumm, A. Arnold, R. Heidinger, M. Rohde, R. Schwab, and R. Spoerl, "Status report on CVD-diamond window development for high power ECRH," *Fusion Eng. Des.*, vol. 53, no. 1–4, pp. 517–524, 2001.

[20] A. Krupnov, M. Tretyakov, V. Parshin, V. Shanin, and S. Myasnikova, "Modern millimeter-wave resonator spectroscopy of broad lines," *J. Mol. Spectrosc.*, vol. 202, no. 1, pp. 107–115, Jul. 2000.

[21] R. Schwab, E. Gaganidze, J. Halbritter, R. Heidinger, R. Aidam, and R. Schneider, "YBCO wafer qualification by surface resistance measurements combined with performance studies of microstrip resonators," *Physica C: Supercond. Appl.*, vol. 351, no. 1, pp. 25–28, 2001.

[22] D. Grischkowsky, S. Keiding, M. Exter, and C. Fattinger, "Far-infrared time-domain spectroscopy with terahertz beams of dielectrics and semiconductors," *J. Opt. Soc. Amer. B*, vol. 7, no. 10, pp. 2006–2015, 1990.

[23] P. Bolivar, M. Brucherseifer, J. Rivas, R. Gonzalo, I. Ederra, A. Reynolds, M. Holker, and P. de Maagt, "Measurement of the dielectric constant and loss tangent of high dielectric-constant materials at terahertz frequencies," *IEEE Trans. Microwave Theory and Techniques*, vol. 51, no. 4, pp. 1062–1066, Apr. 2003.

[24] A. Elhawil, L. Zhang, J. Stiens, C. De Tandt, N. A. Gotzen, G. V. Assche, and R. Vounckx, "A quasi-optical free-space method for dielectric constant characterization of polymer materials in mm-wave band," in *Proc. Symp. IEEE/LEOS Benelux Chapter Brussels*, 2007, pp. 187–190.

[25] T. Jeon and D. Grischkowsky, "Characterization of optically dense, doped semiconductors by reflection THz time domain spectroscopy," *Appl. Phys. Lett.*, vol. 72, no. 23, p. 3032, 1998.

[26] T. Nagashima and M. Hangyo, "Measurement of complex optical constants of a highly doped si wafer using terahertz ellipsometry," *Appl. Phys. Lett.*, vol. 79, no. 24, pp. 3917–3919, Dec. 2001.

[27] N. Matsumoto, T. Hosokura, T. Nagashima, and M. Hangyo, "Measurement of the dielectric constant of thin films by terahertz time-domain spectroscopic ellipsometry," *Optics Lett.*, vol. 36, no. 2, pp. 265–267, Jan. 2011.

[28] A. E. Siegman, *Lasers*. Sausalito, CA: University Science Books, Jan. 1986.

[29] K. Naeli and O. Brand, "An iterative curve fitting method for accurate calculation of quality factors in resonators," *Rev. Sci. Instrum.*, vol. 80, no. 4, p. 045105, 2009.

[30] H. Liebe, "MPM-an atmospheric millimeter-wave propagation model," *Int. J. Infrared and Millim. Waves*, vol. 10, no. 6, pp. 631–50, Jun. 1989.

[31] C. A. Balanis, *Advanced Engineering Electromagnetics*. Hoboken, NJ: Wiley, May 1989.

[32] J. F. Shackelford and W. Alexander, *CRC Materials Science and Engineering Handbook*. Boca Raton, FL: CRC Press, 2001.

[33] P. K. Yu and A. L. Cullen, "Measurement of permittivity by jeans of an open resonator. I. Theoretical," in *Proc. Roy. Soc. London. Series A, Math. Phys. Sci.*, 1982, vol. 380, no. 1778, pp. 49–71.
[34] K. Willis, J. Ayubi-Moak, S. Hagness, and I. Knezevic, "Global modeling of carrier-field dynamics in semiconductors using EMC-FDTD," *J. Computat. Electron.*, vol. 8, no. 2, pp. 153–171, 2009.
[35] K. Willis, S. Hagness, and I. Knezevic, "Terahertz conductivity of doped silicon calculated using the ensemble Monte Carlo/finite-difference time-domain simulation technique," *Appl. Phys. Lett.*, vol. 96, no. 6, p. 062106, 2010.
[36] K. J. Willis, S. C. Hagness, and I. Knezevic, "Multiphysics simulation of high-frequency carrier dynamics in conductive materials," *J. Appl. Phys.*, vol. 110, no. 6, p. 063714, Sep. 2011.
[37] T. I. Jeon and D. Grischkowsky, "Nature of conduction in doped silicon," *Phys. Rev. Lett.*, vol. 78, no. 6, pp. 1106–1109, 1997.
[38] N. W. Ashcroft and N. D. Mermin, *Solid State Physics*, 1st ed. Florence, KY: Brooks/Cole, Jan. 1976.
[39] M. Saillard and D. Maystre, "Scattering from metallic and dielectric rough surfaces," *J. Opt. Soc. Amer. A*, vol. 7, no. 6, pp. 982–990, Jun. 1990.
[40] S. Myasnikova, A. Bogdashov, V. Parshin, and Y. Rodin, "Metal reflectivity investigation at 120–140 GHz," in *4th Int. Kharkov Symp. on Phys. Eng. Millim. Sub-Millim. Waves*, 2001, vol. 2, pp. 857–859.

Benjamin B. Yang (S'02–M'12) received the B.S. degree in mathematics in 2005, and the B.S. and M.S. degrees in electrical engineering in 2005 and 2006, respectively, from the University of Utah, and the Ph.D. degree in electrical engineering from the University of Wisconsin-Madison, in 2011.

In 2002, he was a lab technician at the University of Utah's HEDCO cleanroom facility. From 2003 to 2005, he was an NSF IGERT fellow at the University of Utah. During his time at the University of Wisconsin-Madison, he held various teaching assistant and research assistant positions. He also completed a summer internship at L-3 Communications, Electron Devices in 2006. Since July 2011, he has been with the Validation and Failure Analysis Department at Sandia National Laboratories, Albuquerque, NM. His past and current research interests include terahertz system engineering, nonlinear optics, microelectromechanical systems, and failure analysis and reliability techniques for next-generation integrated circuits, photovoltaic and power electronics technologies.

Dr. Yang is also a member of ASM International and the Electronic Device Failure Analysis Society. His recognitions include the 2011 IEEE International Conference on Plasma Science best student paper award, the Gerald Holdridge Teaching Excellence Award at the University of Wisconsin-Madison, and the Engineering Service Scholar Award at the University of Utah.

Sarah L. Katz received the B.S. degree in physics from Beloit College, Beloit, WI, in 2007, and the M.S. degree in electrical engineering from the University of Wisconsin-Madison, in 2010.

She is currently an Edison Engineer at General Electric's Global Research Laboratory, Niskayuna, NY. Previously, she interned at the Naval Research Lab in Washington, DC, for three summers. Her current research is in silicon carbide power electronic devices, and in the past she has worked on X-ray sources, microwave and plasma processing of metal powders, terahertz resonators, and silicon carbide crystal structure characterization.

Ms. Katz is a member of the American Physical Society.

Keely J. Willis, photograph and biography not available at time of publication.

Marcus J. Weber (M'10) received the B.S. degree in electrical engineering from the University of Wisconsin-Madison in 2012, and is currently working toward the Ph.D. degree from Stanford University, Palo Alto, CA.

In 2008, he was a software engineering intern at GE Healthcare. He also participated in three cooperative education semesters at NASA Johnson Space Center from 2009 to 2011. Additionally, he has worked as an undergraduate researcher since 2010. His research interests are broad and include next generation solid-state devices, high-frequency research and applications, and optoelectronics.

Mr. Weber received both the Stanford Graduate Fellowship and the NSF Graduate Research Fellowship. He is also a member of the Tau Beta Pi and has received various undergraduate academic awards, including the Polygon Outstanding Senior Award.

Irena Knezevic (S'02–M'04) received the B.S. degree in theoretical physics from the University of Belgrade, Serbia, in 1995, and the Ph.D. degree in electrical engineering from Arizona State University in 2004.

She joined the faculty of the Electrical and Computer Engineering Department at the University of Wisconsin, Madison, as an Assistant Professor in 2004, and was promoted to Associate Professor in 2010. She has published over 50 peer-reviewed journal papers and contributed toward more than 120 conference papers and presentations. Her research activities focus on quantum and semiclassical simulation of carrier transport in electronic and optoelectronic semiconductor devices, as well as on heat transport at the nanoscale and nanostructured thermoelectrics.

Dr. Knezevic is a recipient of the 2004–2005 Palais' Oustanding Doctoral Student Award, the 2006 NSF Early Career Development (NSF CAREER) award, the 2009 AFOSR Young Investigator Research Program (YIP) Award, as well as the 2011 James G. Woodburn Award for Excellence in Undergraduate Teaching. She is an associate editor of the *Journal of Computational Electronics*, and served as the general chair or the 2012 15th International Workshop on Computational Electronics (IWCE 2012). She is a member of the American Physical Society.

Susan C. Hagness (S'91–M'98–SM'04–F'09) received the B.S. degree (with highest honors) and the Ph.D. degree in electrical engineering from Northwestern University, Evanston, IL, in 1993 and 1998, respectively. While pursuing the Ph.D. degree, she was a National Science Foundation (NSF) Graduate Fellow and a Tau Beta Pi Spencer Fellow.

Since August 1998, she has been with the Department of Electrical and Computer Engineering at the University of Wisconsin-Madison, where she currently holds the title of Philip D. Reed Professor. She is also a faculty affiliate of the Department of Biomedical Engineering. Her current research interests include bioelectromagnetics, microwave inverse scattering, microwave thermotherapy, nanoparticles as electromagnetic theranostic agents, electric-field-mediated gene and drug delivery at the cellular level, time-domain computational electromagnetics theory and applications, and multiphysics numerical simulation of high-frequency field-carrier dynamics in conducting materials.

Dr. Hagness served as an elected member of the IEEE Antennas and Propagation Society (AP-S) Administrative Committee from 2003 to 2005 and as an Associate Editor for the IEEE ANTENNAS AND WIRELESS PROPAGATION LETTERS from 2002 to 2007. She is currently serving as Vice-Chair of the IEEE AP-S Fellows Committee, a member of the IEEE AP-S Awards Committee, and the Technical Program Chair of the 2012 IEEE International Symposium on Antennas and Propagation and USNC/URSI National Radio Science Meeting. She was the recipient of the Presidential Early Career Award for Scientists and Engineers presented by the White House in 2000. In 2002, she was named one of the 100 top young innovators in science and engineering in the world by the Massachusetts Institute of Technology (MIT) Technology Review magazine. She is also the recipient of the UW-Madison Emil Steiger Distinguished Teaching Award (2003), the IEEE Engineering in Medicine and Biology Society Early Career Achievement Award (2004), the URSI Isaac Koga Gold Medal

(2005), the IEEE Transactions on Biomedical Engineering Outstanding Paper Award (2007), the IEEE Education Society's Mac E. Van Valkenburg Early Career Teaching Award (2007), the UW System Alliant Energy Underkofler Excellence in Teaching Award (2009), the UW-Madison Kellett Mid-Career Award (2011), and the Physics in Medicine and Biology Citations Prize and Rotblat Medal (2011).

John H. Booske (S'82–M'85–SM'93–F'07) received the Ph.D. degree in nuclear engineering from the University of Michigan, Ann Arbor, in 1985.

From 1985 to 1989, he was a Research Scientist with the University of Maryland, College Park, researching magnetically confined hot ion plasmas and sheet-electron-beam free electron lasers. Since 1990, he has been with the faculty of the Department of Electrical and Computer Engineering, University of Wisconsin, Madison (UW), where he is currently the Chair of the department, Director of the Wisconsin Collaboratory for Enhanced Learning (a learning space that supports IT-assisted, peer-collaborative learning) and the Duane H. and Dorothy M. Bluemke Professor of Engineering. From 2001 to 2005, he served as Director of the UW Interdisciplinary Materials Science Program. His research interests include experimental and theoretical study of coherent electromagnetic radiation, its sources and its applications, spanning the RF, microwave, millimeter-wave, and THz regimes. His recent research activities include vacuum electronics, microfabrication of millimeter-wave and THz regime sources and components, high-power microwaves, advanced cathodes, physics of the interaction of THz radiation and materials, microwave-generated plasma discharges and biological applications of electric and electromagnetic fields. He was a coeditor of *Microwave and Radio Frequency Applications* (American Ceramic Society, 2003) and *Microwave and Millimeter-Wave Power Electronics* (IEEE/Wiley, 2005).

Professor Booske has been a Guest Editor of the IEEE TRANSACTIONS ON PLASMA SCIENCE. He received the University of Wisconsin Vilas Associate Award for research and the U.S. National Science Foundation Presidential Young Investigator Award. He has received many teaching awards, including the UW Chancellor's Distinguished Teaching Award. He is a Fellow of the American Physical Society.